

Effect of C₆₀ nanoparticles on elasticity of small unilamellar vesicles composed of DPPC bilayers*

Tanlin Wei(魏坦琳), Lei Zhang(张蕾)[†], and Yong Zhang(张勇)[‡]

School of Physics, Sun Yat-Sen University, Guangzhou 510275, China

(Received 16 January 2020; revised manuscript received 19 February 2020; accepted manuscript online 9 March 2020)

The interaction between C₆₀ nanoparticles and biomembranes has been of great interest in researches over the past decades due to their novel applications as well as potential cytotoxicity. In this work, we study the deformation of the small unilamellar vesicles composed of dipalmitoylphosphatidylcholine (DPPC) lipid bilayers infiltrated with C₆₀ nanoparticles of different molecular concentrations through coarse-grained molecular dynamics simulations. By employing the Helfrich spontaneous curvature model, the bending modulus and the spontaneous curvature of the vesicles with C₆₀ nanoparticles of different concentrations are obtained according to the simulation data. The results show that the bending modulus and the spontaneous curvature of pure DPPC vesicle membranes are approximately 1.6×10^{-19} J and 1.4 nm^{-1} , respectively. Both of them increase linearly approximately as the C₆₀ concentration increases from 0 to 16.3%. The density profiles of vesicles, the order of lipid packing and the diffusion characteristics of DPPC and C₆₀ are also investigated.

Keywords: lipid vesicle, bending modulus, C₆₀ nanoparticles, spontaneous curvature

PACS: 87.15.ap, 87.16.D-, 87.15.La, 87.10.Pq

DOI: 10.1088/1674-1056/ab7d9f

1. Introduction

In the past decades, nanomaterials have been developed rapidly due to their remarkable physical and chemical characteristics and numerous potential applications in the biological and medical fields.^[1-4] Among these nanomaterials, fullerenes, including functional C₆₀, C₆₀ derivatives and polymer/C₆₀ composites, have attracted massive attention.^[5,6] Those C₆₀ nanomaterials exhibit crucial physicochemical properties like solubility in diverse solvents, redox properties, optic properties, *etc.*^[5-7] Therefore, they are candidates for such hopeful biomedical applications as anti-oxidation, enzyme inhibition, antiviral activity, electron transfer and photodynamic therapy.^[5-7] Despite a broad and fascinating prospect of C₆₀ in biomedicine, they potentially lead to cytotoxicity.^[8-10] Cases in point are studies about C₆₀ causing oxidative damage to cell membranes,^[11,12] changing the morphology of vascular endothelial cells,^[13] inhibiting cell differentiation and suppressing cell proliferation.^[14,15] Consequently, it is necessary to investigate the interaction between C₆₀ and cells for biomedical applications.

Biomembranes play an indispensable role in many important functions of cells. Although biomembranes are complexes of various types of molecules, they all consist of a lipid bilayer serving as a backbone for membrane proteins and carbohydrates.^[16,17] Usually, the bilayer containing only one kind of lipid molecules is employed as a simplified model in the study of biomembranes. Due to the amphipathic character of lipids, the lipid bilayer in water could assemble spontaneously into a unilamellar vesicle, which is employed as a

simple model of cell in the literature.^[18-21] In recent years, it has been found that vesicles could be taken as the nano-encapsulation agents for medicine.^[22-24]

Investigating the mechanic effects of C₆₀ on biomembranes (*e.g.*, the alteration to rigidity) are vital for understanding its cytotoxicity and targeted drug delivery.^[25-28] Zhang and co-workers concluded experimentally that C₆₀ nanoparticles make human red blood cell membranes softer.^[29] Drasler *et al.* reported a drop in the bending rigidity of POPC bilayers by the addition of 10% of C₆₀.^[30] Meanwhile, Skorkina *et al.* found that the aqueous solution with the C₆₀ concentration of 0.1 mg/ml can increase the stiffness of the lymphocyte membrane by 41%.^[31] In addition, Zhou *et al.* revealed that the incorporation of C₆₀ with a molar concentration of 0.8% can increase Young's modulus of gel phase lipid bilayers, but barely changes that of fluid phase bilayers.^[32]

On the other hand, molecular dynamics (MD) simulations showed that C₆₀ molecules are capable of translocating to the internal region of lipid bilayers spontaneously, affecting the structures and mechanic properties of plane membranes as well as inducing the dynamic interactions.^[33-40] Wong-Ekkabut *et al.* carried out a simulation study on a plane lipid membrane and concluded that C₆₀ with a concentration lower than 10% alters the elasticity of lipid bilayers, but is not enough to mechanically disrupt the membranes.^[41] Recently, Xie *et al.* suggested that the initial aggregation state of C₆₀ has an influence on the interactions between C₆₀ and lipid bilayers: small C₆₀ clusters expand the area and thickness of plane membranes while large ones decrease the membrane area by

*Project supported by the National Natural Science Foundation of China (Grant No. 61475196).

[†]Corresponding author. E-mail: zhlei28@mail.sysu.edu.cn

[‡]Corresponding author. E-mail: zhyong9@mail.sysu.edu.cn

© 2020 Chinese Physical Society and IOP Publishing Ltd

<http://iopscience.iop.org/cpb> <http://cpb.iphy.ac.cn>

the protrusion of lipids.^[42]

The shapes of closed vesicles are well described by the Helfrich spontaneous curvature model.^[43] Accordingly, the elastic energy E of a closed vesicle is

$$E = \frac{\kappa_c}{2} \iint (C_1 + C_2 - C_0)^2 dA, \quad (1)$$

where κ_c represents the bending modulus, C_1 and C_2 are the principal curvatures, C_0 is the spontaneous curvature.^[44] As for open vesicles with free edges, Tu and Ou-Yang obtained the total free energy of the surface and the boundary curve, and derived the equilibrium equation and the boundary conditions of biomembranes.^[45] Tu also discussed the compatibility between the shape equation and the boundary conditions.^[46] Recently, Zhou studied the boundary behaviors of open vesicles in the axisymmetric case to look into the continuous transformation from a closed vesicle to an open vesicle.^[47] In the present work, we consider closed vesicles only. In the following, we refer to closed vesicles simply as vesicles.

The bending modulus and the spontaneous curvature are critical parameters evaluating the elastic properties of lipid bilayers quantitatively. So far, there have been some researches on measuring the bending modulus of simple lipid bilayers through simulations or experiments. However, the obtained values are not consistent.^[48–60] Moreover, few researches have determined the spontaneous curvature.^[51,56] Venable *et al.* utilized the method of thermal fluctuations to calculate the bilayer bending modulus and the monolayer spontaneous curvature of pure lipid bilayers through MD simulations.^[59] Nevertheless, they did not obtain the spontaneous curvature of bilayer directly.

In this work, we employ the Helfrich spontaneous curvature model to obtain the dependence of the bending modulus and the spontaneous curvature of dipalmitoylphosphatidylcholine (DPPC) lipid vesicles on the concentration of C_{60} nanoparticles through MD simulations. The results show that the infiltration of C_{60} nanoparticles into the vesicles increases the bending modulus and the spontaneous curvature linearly approximately. Furthermore, other structural and dynamic properties of the vesicles with C_{60} infiltration are studied to explain the elastic alteration.

2. Methods

2.1. Simulation methodology

The MD simulations were performed through Gromacs 5.1.1,^[61–63] using the Martini coarse-grained (CG) force field.^[64,65] The visual images were produced by VMD 1.9.3.^[66] The Martini CG models of DPPC and C_{60} are shown in Fig. 1.

The lipid vesicle used in the current simulations was generated by Martini Vesicle Maker of CHARMM.^[67,68] A lipid vesicle was placed in a cubic simulation box with a side

length of 24.5 nm. Each simulation box contains 2637 DPPC molecules and 95252 CG water beads. The system was equilibrated at the temperature of 303 K and the isotropic pressure of 1.0 bar (ambient pressure p_0).

The coordinate file of a single C_{60} molecule was extracted from the website of Martini force field (<http://cgmartini.nl/index.php/example-applications2>). C_{60} molecules were inserted into the aqueous solution of pure DPPC vesicle and located randomly in the beginning to prepare the systems with different C_{60} molecular concentrations, noted as $c(C_{60})$, varying from 0 to 16.3%. Each of these systems was equilibrated at 303 K and ambient pressure until all C_{60} molecules spontaneously entered the internal region of the DPPC bilayer.

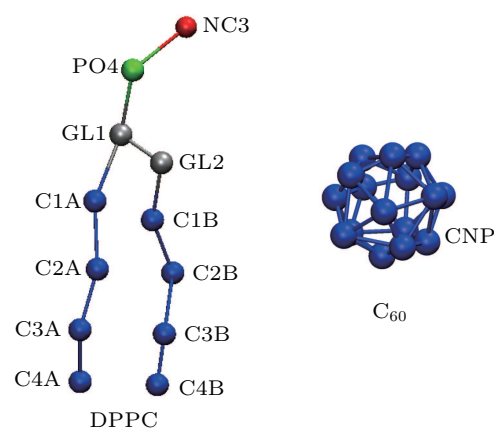


Fig. 1. CG molecular representations of DPPC and C_{60} . A DPPC molecule consists of 12 CG beads labeled by names and colors. A C_{60} molecule consists of 16 CNP CG beads.

For each of the equilibrated C_{60} -vesicle systems, the dynamic simulations were performed applying a semi-isotropic pressure coupling in three-dimensional Cartesian rectangular coordinates. In this way, the components of the mechanic stress along x and y directions (horizontal direction) maintained ambient pressure, while the component along z direction (vertical direction) was assigned as 4.0, 8.0, 12.0, 16.0, and 20.0 bar, respectively. The constant pressure was implemented by the Berendsen scheme with a coupling constant of 5.0 ps. The temperature was constantly set at 303 K by the velocity-rescaling scheme with a coupling constant of 1.0 ps. Both the electrostatic cut-off and the van der Waals cut-off were at 1.1 nm. The time step of simulations was 30 fs.

The systems were regarded to achieve equilibrium when the side length of the system boxes remained stable relatively. Then the simulations were terminated. In our case, each simulation of the semi-isotropic pressure coupling was run for 300 ns.

2.2. Theoretic model of the elastic deformation

As a consequence of the vertical pressure, the initially spherical vesicle will deform. According to the simulations, the deformed vesicle can be abstracted into a geometry consisting of a rotationally symmetric side surface and two round

planes at top and bottom, depicted in Fig. 2. It should be emphasized that the shape shown in Fig. 2 is not a solution to the equilibrium shape equation obtained by Ou-Yang and Helfrich in 1987.^[69] The length parameters L and R (annotated in Fig. 2) are parameters describing the shape of vesicle.

At a constant temperature, the exchange of molecules between the membrane and the solution is negligible, and the membrane is hardly stretchable.^[43] Thus, the area of the vesicle membrane during pressurization is assumed to be a constant. Accordingly, L is represented as a function of R ,

$$L = \frac{-\pi R + \sqrt{\pi^2 R^2 + 8(R_0^2 - R^2)}}{2}, \quad (2)$$

where R_0 is the radius of the initial spherical vesicle. Therefore, R is the only independent parameter characterizing the shape of the deformed vesicle.

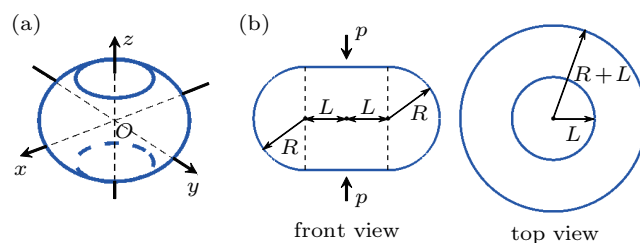


Fig. 2. Geometric model of the deformed vesicle. The vesicle is abstracted into a geometry consisting of a rotationally symmetric side surface and two round planes at top and bottom. (a) Three-dimensional view. A fixed global right-handed Cartesian coordinate system is set up, with its origin labeled as O , at the center of the vesicle. (b) Front view and top view. In the front view, the outline of the vesicle is constituted by two horizontal straight lines with length $2L$, and two semicircles with radius R . The vertical pressure p is along the z axis. In the top view, there appear conceivably two concentric circles with radius L and $R+L$, respectively.

One can obtain the elastic energy of the vesicle based on the Helfrich spontaneous curvature model

$$E = \begin{cases} 2\pi\kappa_c(2 - C_0R_0)^2, & R = R_0, \\ \frac{\pi\kappa_c}{R} \left[(2R + \pi L)(2 - C_0R)^2 - 2\pi L(2 - C_0R) + L^2 \int_0^\pi \frac{d\theta}{L+R\sin\theta} \right] + \pi\kappa_c C_0^2 L^2, & 0 < R < R_0. \end{cases} \quad (3)$$

On the other hand, one has

$$-2p\pi L^2 = \frac{dE}{dR}, \quad (4)$$

where p is the vertical pressure.

Using Eqs. (2), (3), and (4), we can obtain the bending modulus and the spontaneous curvature by fitting the simulation data.

3. Results and discussion

3.1. Bending modulus and spontaneous curvature of the vesicle membranes with different C_{60} concentrations

The typical deformation of vesicles under different vertical pressures at equilibrium is shown in Fig. 3(a). The deformation of the vesicles with C_{60} nanoparticles of different

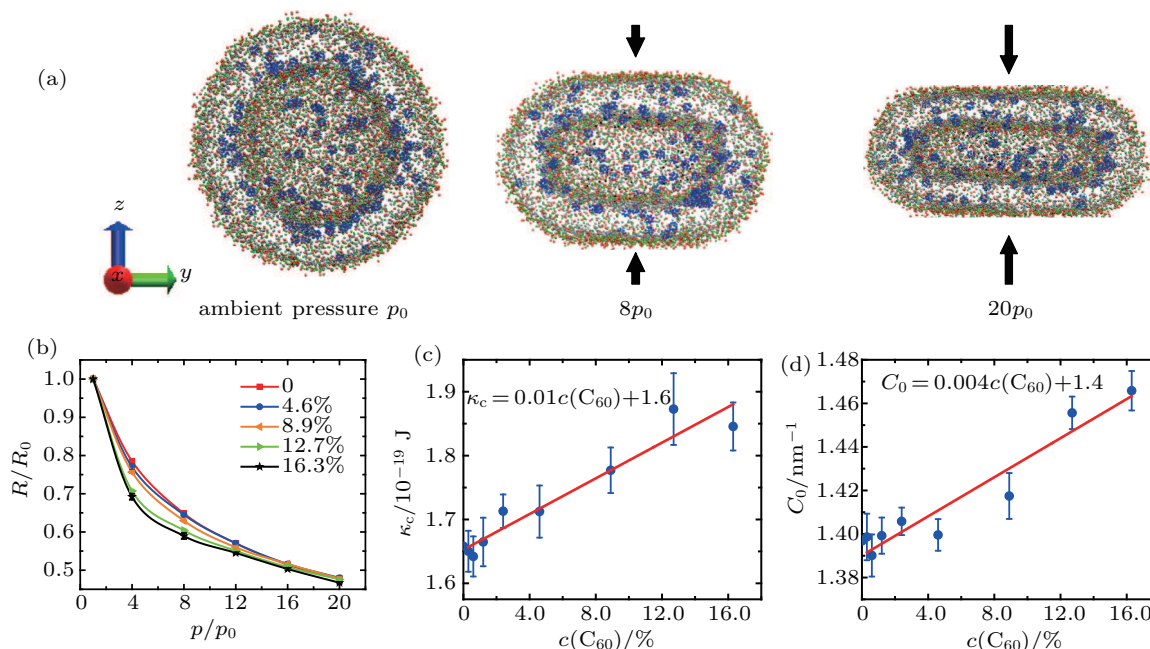


Fig. 3. (a) Deformation of the vesicle under vertical pressures. Plotted is the front view of the vesicle with the C_{60} concentration of 4.6% at equilibrium. The first vesicle is the initial spherical one. The second and third ones are under the vertical pressures of $8p_0$ and $20p_0$, respectively. Color code as used in Fig. 1. Water and carbohydrate tails of lipids are not shown for clarity. (b) The relation between the geometric parameter R of the vesicle with different C_{60} concentrations and the vertical pressure. The vertical pressure p is scaled by ambient pressure p_0 , and R is normalized by the radius of the initial vesicle R_0 . (c) Dependence of the bending modulus of DPPC bilayer on the C_{60} concentration. (d) Dependence of the spontaneous curvature of DPPC bilayer on the C_{60} concentration. In (c) and (d), symbols are the results from our simulations, and solid lines indicate linear fitting with the equations aside.

molecular concentrations under various vertical pressures are quantitatively described by R vs. p , plotted in Fig. 3(b).

The bending modulus κ_c and the spontaneous curvature C_0 of the vesicle membranes are obtained by fitting our simulation data to Eqs. (2), (3), and (4) in the least-squares sense. The results are shown in Figs. 3(c) and 3(d).

Our results show that the bending modulus of the pure DPPC vesicle membrane is approximately 1.6×10^{-19} J, roughly in agreement with the values obtained in previous simulations and experiments.^[49,52,53,55,58,59,70] It is suggested that our simulations and theoretic analyses should be reliable, though the size of vesicle used in our simulations is not so large that the thickness of membrane can be neglected. The bending modulus increases linearly approximately as the C_{60} concentration increases from 0 to 16.3%.

The spontaneous curvature of the pure DPPC vesicle membrane is 1.4 nm^{-1} . It also increases linearly approximately with the increasing C_{60} concentration.

3.2. Size and structural properties of the vesicles: density profiles

The density profiles of DPPC, water and C_{60} in the vesicles at different vertical pressures and C_{60} concentrations are shown in Fig. 4(a).

According to the radial density profiles (density vs distance from the center of the spherical vesicle, r_0) under ambient pressure (Fig. 4(a), 1st row), C_{60} nanoparticles tend to distribute in the inner leaflet of DPPC bilayer more than in the outer leaflet. The peak of the DPPC density curve reduces and the width increases with the increase of C_{60} . Moreover, the inner leaflet shows a lower peak compared with the outer leaflet as C_{60} nanoparticles infiltrate into the membrane.

The density profiles under pressurization are depicted by the density distributions along the z axis (Fig. 4(a), 2nd and 3rd rows) and the radial density distributions in the xy plane (Fig. 4(a), 4th and 5th rows). From the density profiles under pressurization, one can notice the similar phenomena to that from the density profiles under ambient pressure.

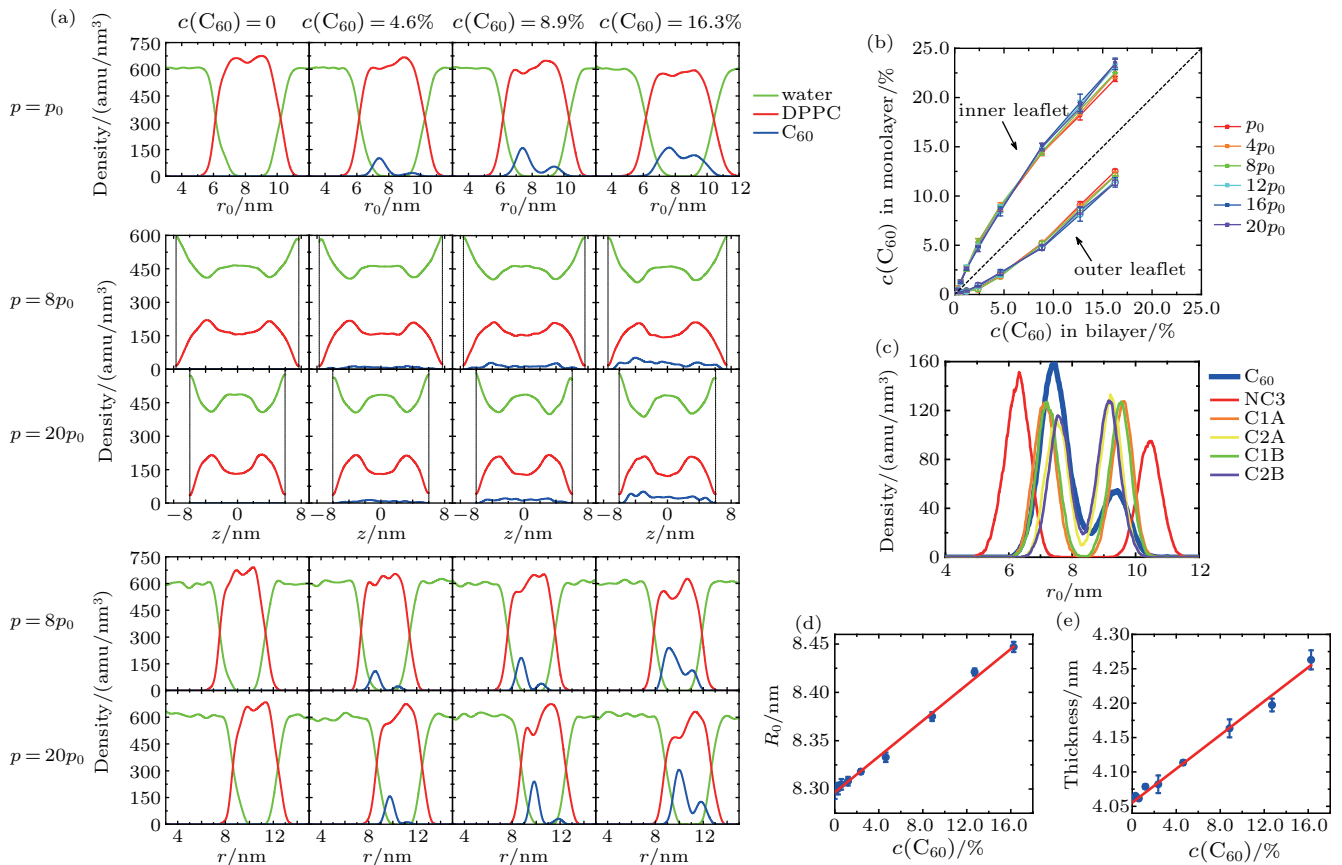


Fig. 4. (a) Density profiles of water, DPPC and C_{60} in the vesicles at different vertical pressures (annotated on the left) and C_{60} concentrations (annotated at top). The radial density profiles under ambient pressure (1st row) are depicted by density vs distance from the center of the spherical vesicle, r_0 . The density profiles under pressurization are depicted by the density distributions along the z axis (2nd and 3rd rows, where the vertical dashed lines indicate the boundary of systems) and the radial density distributions in the xy plane (4th and 5th rows, where r is the distance from the center of the vesicle in the xy plane). (b) Distribution of C_{60} concentration in the inner (solid cubic symbols, all above the dashed line) and outer (open circle symbols, all below the dashed line) leaflets at different vertical pressures and total concentrations in the bilayers, plotted with the solid lines as guides to the eyes. The dashed black line with a slope of 1 is drawn as a reference. (c) Radial density profiles of some CG beads under ambient pressure in the system with C_{60} concentration of 8.9%. (d) Radius of the initial vesicles as a function of the C_{60} concentration. (e) Thickness of DPPC bilayers as a function of the C_{60} concentration. In (d) and (e), symbols are the measured data from our simulations, and solid lines indicate the results of linear fitting.

The C_{60} concentrations in the inner leaflet and the outer leaflet are quantitatively measured (Fig. 4(b)). As the total concentration of C_{60} in the bilayer and the vertical pressure vary, the concentration in the inner leaflet (Fig. 4(b), above the dashed reference line) is always larger than that in the outer leaflet (Fig. 4(b), below the dashed reference line). The uneven distribution of C_{60} may be attributed to the fact that the curvature of the inner leaflet is larger than that of the outer one, so there is more room for nanoparticles near lipid tails in the inner leaflet.

The radial density profiles of some CG beads under ambient pressure are illustrated in Fig. 4(c). C_{60} nanoparticles are inclined to distribute near the first two beads of carbohydrate tails, as a probable consequence of the atomic interaction between the constituents of C_{60} and DPPC.

Additionally, the infiltration of C_{60} into the bilayer changes the size of the vesicle membrane. Both the radius of the initial spherical vesicle and the thickness of DPPC bilayer

increase linearly with the C_{60} concentration (see in Figs. 4(d) and 4(e)).

3.3. Structural properties of the vesicles: order of lipid packing

The angle between two carbohydrate tails of the lipid is chosen as the order parameter.^[71] The tail angle distributions of membranes at diverse vertical pressures and C_{60} concentrations are illustrated in Fig. 5(a). In a vesicle, the tail angle distribution of the inner leaflet (Fig. 5(a), red curve) is broader and has a peak farther from 0° than that of the outer leaflet (Fig. 5(a), blue curve). Nevertheless, as the C_{60} concentration in the bilayer increases, the angle distributions of the inner and the outer leaflet tend to coincide. In addition, the angle distributions of bilayer (Fig. 5(a), black curve) and two monolayers are broader and have peaks farther from 0° at a lower C_{60} concentration or under a higher vertical pressure.

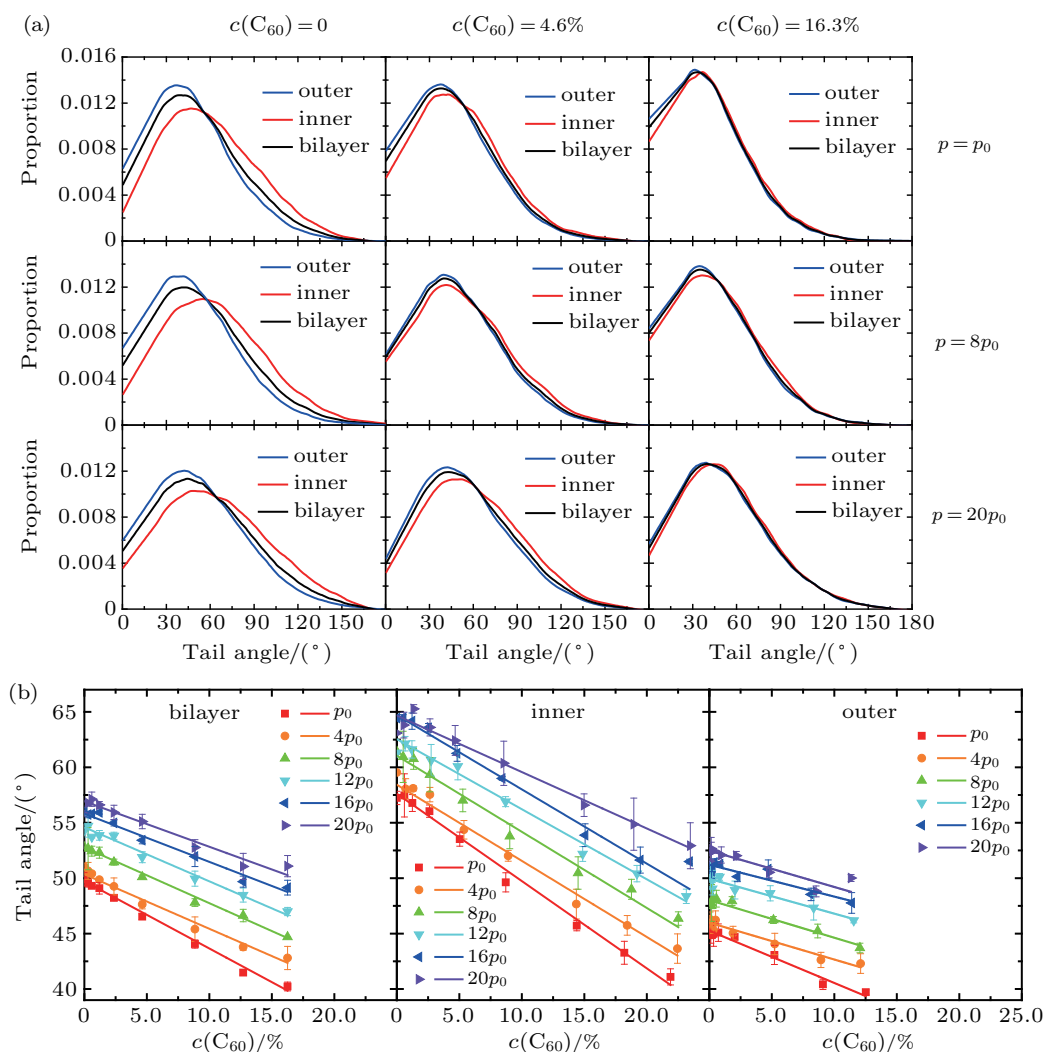


Fig. 5. (a) Tail angle distributions of the vesicles with various C_{60} concentrations (annotated at top) under diverse vertical pressures (annotated on the right). (b) Relation between the average of tail angles in the membrane and the C_{60} concentration under different pressures, presented separately for the bilayer and each monolayer. Symbols are the measured data from our simulations, and solid lines indicate the results of linear fitting to each set of data.

The average of tail angles in the membrane is calculated, seen in Fig. 5(b). The tail angle averages of bilayer (Fig. 5(b), left) and two monolayers (Fig. 5(b), middle and right) all decrease with the increasing C_{60} concentration in the layer. They increase with the increasing vertical pressure.

The broader distribution with a peak farther from 0° suggests that the packing of lipids is less ordered. Similarly, the smaller average of tail angles means the higher order of the vesicle membrane. Altogether, we could draw three conclusions: in a vesicle, the lipid packing is less ordered in the inner leaflet than in the outer leaflet, but the difference in lipid packing between the two monolayers becomes less obvious as more C_{60} nanoparticles enter the bilayer; the vertical pressurization forces the vesicle membranes into a more disordered state; the infiltration of C_{60} enhances the order of lipid packing.

3.4. Dynamic properties of the vesicles: molecular diffusion coefficients

The diffusion coefficients of DPPC molecules and C_{60} nanoparticles in the vesicles under ambient pressure are shown in Fig. 6. In a vesicle, C_{60} nanoparticles diffuse more slowly than DPPC molecules. The diffusion coefficients of lipids and C_{60} in the vesicle are in the range of the values obtained by previous simulations on the plane membranes.^[36,39,41,72,73] Both the diffusion coefficient of DPPC and that of C_{60} descend on the whole as the C_{60} concentration in the vesicle increases. This means that the fluidity of the membrane becomes worse.

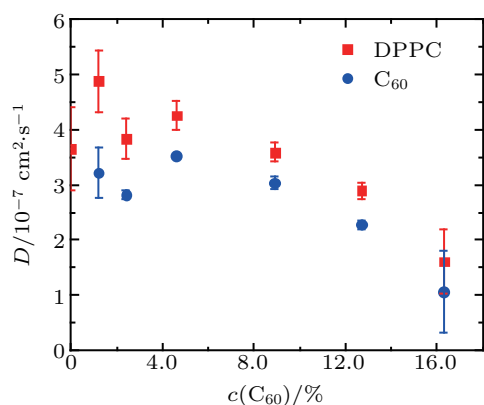


Fig. 6. Diffusion coefficients of DPPC molecules and C_{60} nanoparticles in the vesicles with different C_{60} concentrations under ambient pressure.

3.5. Discussion

According to our simulations and analyses, the native structures of vesicles and the atomic interaction between C_{60} and lipids affect the spontaneous infiltration and the uneven distribution of C_{60} in the bilayers. The infiltration and distribution of C_{60} nanoparticles, in turn, alter the sizes, the structural and the dynamic properties of the vesicles. The modulation of structures and dynamics has an further influence on the elasticity of the vesicles. On the one hand, C_{60} nanoparticles

induce the order of lipid packing, reduce the fluidity of membranes, then strengthen the vesicle, and increase the bending modulus. On the other hand, C_{60} nanoparticles change the asymmetry between the two monolayers of the bilayer (*i.e.*, the infiltration of C_{60} modifies the density profiles and the tail angle distributions of inner and outer leaflets), and thus alter the spontaneous curvature of the vesicle membrane.

4. Conclusion

We have explored the effect of C_{60} nanoparticle infiltration on the vesicles composed of DPPC lipid bilayers through CG MD simulations. The bending modulus and the spontaneous curvature of the DPPC vesicles with C_{60} nanoparticles of different molecular concentrations have been obtained based on the Helfrich spontaneous curvature model. The bending modulus and the spontaneous curvature of pure DPPC vesicles are approximately 1.6×10^{-19} J and 1.4 nm^{-1} , respectively. It is concluded that both the bending modulus and the spontaneous curvature increase linearly approximately with the C_{60} concentration (0–16.3%).

References

- [1] Xia Y 2008 *Nat. Mater.* **7** 758
- [2] Mitragotri S and Lahann J 2009 *Nat. Mater.* **8** 15
- [3] Zeng Y H, Jiang W G and Qin Q H 2016 *Acta Phys. Sin.* **65** 148802 (in Chinese)
- [4] Li R, Liu T, Chen X, Chen S C, Fu Y H and Liu L 2018 *Acta Phys. Sin.* **67** 190202 (in Chinese)
- [5] Kausar A 2017 *Polym.-Plast. Technol. Eng.* **56** 594
- [6] Rašović I 2017 *Mater. Sci. Technol.* **33** 777
- [7] Jensen A W, Wilson S R and Schuster D I 1996 *Bioorganic & Medicinal Chemistry* **4** 767
- [8] Nel A, Xia T, Mädler L and Li N 2006 *Science* **311** 622
- [9] Powell M C and Kanarek M S 2006 *Wisconsin Med. J.* **105** 18
- [10] De Jong W H and Borm P J 2008 *Int. J. Nanomedicine* **3** 133
- [11] Sayes C M, Fortner J D, Guo W, Lyon D, Boyd A M, Ausman K D, Tao Y J, Sitharaman B, Wilson L J and Hughes J B 2004 *Nano Lett.* **4** 1881
- [12] Sayes C M, Gobin A M, Ausman K D, Mendez J, West J L and Colvin V L 2005 *Biomaterials* **26** 7587
- [13] Yamawaki H and Iwai N 2006 *Am. J. Physiol.-Cell Physiol.* **290** C1495
- [14] Tsuchiya T, Oguri I, Yamakoshi Y N and Miyata N 1996 *FEBS Lett.* **393** 139
- [15] Sosnowska M, Kutwin M, Jaworski S, Strojny B, Wierzbicki M, Szczepaniak J, Łojkowski M, Świąszkowski W, Bałaban J and Chwalibog A 2019 *Int. J. Nanomedicine* **14** 6197
- [16] Karp G 2009 *Cell and Molecular Biology: Concepts and Experiments* (John Wiley & Sons)
- [17] Li Z L 2018 *Chin. Phys. B* **27** 038703
- [18] Tanford C 1980 *Hydrophobic Effect: Formation Micelles Biological Membranes* 2d edn (New York: Wiley)
- [19] Cevc G and Marsh D 1987 *Phospholipid Bilayers: Physical Principles and Models* (New York: Wiley)
- [20] Li Y and ten Wolde P R 2019 *Phys. Rev. Lett.* **123** 148003
- [21] Stelter D and Keyes T 2019 *Soft Matter* **15** 8102
- [22] Hossann M, Syunyaeva Z, Schmidt R, Zengerle A, Eibl H, Issels R D and Lindner L H 2012 *J. Controlled Release* **162** 400
- [23] May J P and Li S D 2013 *Expert Opinion Drug Delivery* **10** 511
- [24] Fujie T and Yoshimoto M 2019 *Soft Matter* **15** 9537
- [25] Holme M N, Fedotenko I A, Abegg D, Althaus J, Babel L, Favarger F, Reiter R, Tanasescu R, Zaffalon P L, Ziegler A, Müller B, Saxer T and Zumbühl A 2012 *Nat. Nanotechnol.* **7** 536
- [26] Garg S, Thomas A A and Borden M A 2013 *Biomaterials* **34** 6862
- [27] Saxer T, Zumbühl A and Müller B 2013 *Cardiovasc. Research* **99** 328

- [28] Sun J, Zhang L, Wang J, Feng Q, Liu D, Yin Q, Xu D, Wei Y, Ding B and Shi X 2015 *Adv. Mater.* **27** 1402
- [29] Zhang X, Zhang Y, Zheng Y and Wang B 2013 *Phys. Chem. Chem. Phys.* **15** 2473
- [30] Drasler B, Drobne D, Sadeghpour A and Rappolt M 2015 *Chem. Phys. Lipids* **188** 46
- [31] Skorkina M Y, Sladkova E A, Shamray E A, Cherkashina O V, Evstigneev M P, Buchelnikov A S, Prylutskiy Y I and Ritter U 2015 *Eur. Biophys. J.* **44** 493
- [32] Zhou J, Liang D and Contera S 2015 *Nanoscale* **7** 17102
- [33] Li L, Davande H, Bedrov D and Smith G D 2007 *J. Phys. Chem. B* **111** 4067
- [34] Qiao R, Roberts A P, Mount A S, Klaine S J and Ke P C 2007 *Nano Lett.* **7** 614
- [35] Chang R W and Lee J M 2010 *Bull. Korean Chem. Soc.* **31** 3195
- [36] Jusufi A, DeVane R H, Shinoda W and Klein M L 2011 *Soft Matter* **7** 1139
- [37] Zhang S, Mu Y, Zhang J Z and Xu W 2013 *PLoS One* **8** e77436
- [38] Barnoud J, Rossi G and Monticelli L 2014 *Phys. Rev. Lett.* **112** 068102
- [39] Bozdaganyan M E, Orekhov P S, Shaytan A K and Shaitan K V 2014 *PLoS One* **9** e102487
- [40] Atilhan M, Costa L T and Aparicio S 2019 *J. Mol. Liq.* **295** 111714
- [41] Wong-Ekkabut J, Baoukina S, Triampo W, Tang I M, Tieleman D P and Monticelli L 2008 *Nat. Nanotechnol.* **3** 363
- [42] Xie L Q, Liu Y Z, Xi Z H, Li H Y, Liang S D and Zhu K L 2017 *Mol. Simul.* **43** 1532
- [43] Helfrich W 1973 *Z. Naturforsch. C* **28** 693
- [44] Lipowsky R 1999 *Statistical Mechanics of Biocomplexity* (Berlin: Springer) pp. 1–23
- [45] Tu Z and Ou-Yang Z C 2003 *Phys. Rev. E* **68** 061915
- [46] Tu Z 2010 *J. Chem. Phys.* **132** 084111
- [47] Zhou X 2019 *J. Phys.: Condens. Matter* **31** 315101
- [48] Evans E and Rawicz W 1990 *Phys. Rev. Lett.* **64** 2094
- [49] Lindahl E and Edholm O 2000 *Biophys. J.* **79** 426
- [50] Rawicz W, Olbrich K, McIntosh T, Needham D and Evans E 2000 *Biophys. J.* **79** 328
- [51] Döbereiner H G, Gompper G, Haluska C K, Kroll D M, Petrov P G and Riske K A 2003 *Phys. Rev. Lett.* **91** 048301
- [52] Marrink S J, De Vries A H and Mark A E 2004 *J. Phys. Chem. B* **108** 750
- [53] Delorme N and Fery A 2006 *Phys. Rev. E* **74** 030901
- [54] Guler S D, Ghosh D D, Pan J, Mathai J C, Zeidel M L, Nagle J F and Tristram-Nagle S 2009 *Chem. Phys. Lipids* **160** 33
- [55] Picas L, Rico F and Scheuring S 2012 *Biophys. J.* **102** L01
- [56] Bassereau P, Sorre B and Lévy A 2014 *Adv. Colloid Interface Sci.* **208** 47
- [57] Jablin M S, Akabori K and Nagle J F 2014 *Phys. Rev. Lett.* **113** 248102
- [58] Nagle J F, Jablin M S, Tristram-Nagle S and Akabori K 2015 *Chem. Phys. Lipids* **185** 3
- [59] Venable R M, Brown F L and Pastor R W 2015 *Chem. Phys. Lipids* **192** 60
- [60] Faizi H A, Frey S L, Steinkühler J, Dimova R and Vlahovska P M 2019 *Soft Matter* **15** 6006
- [61] Berendsen H J, van der Spoel D and van Drunen R 1995 *Comput. Phys. Commun.* **91** 43
- [62] Van Der Spoel D, Lindahl E, Hess B, Groenhof G, Mark A E and Berendsen H J 2005 *J. Comput. Chem.* **26** 1701
- [63] Abraham M J, Murtola T, Schulz R, Páll S, Smith J C, Hess B and Lindahl E 2015 *Software X* **1** 19
- [64] Marrink S J, Risselada H J, Yefimov S, Tieleman D P and De Vries A H 2007 *J. Phys. Chem. B* **111** 7812
- [65] Periolo X and Marrink S J 2013 *Biomolecular Simulations* (Berlin: Springer) pp. 533–565
- [66] Humphrey W, Dalke A and Schulten K 1996 *J. Molecular Graphics* **14** 33
- [67] Jo S, Kim T, Iyer V G and Im W 2008 *J. Comput. Chem.* **29** 1859
- [68] Qi Y, Ingólfsson H I, Cheng X, Lee J, Marrink S J and Im W 2015 *J. Chem. Theory Comput.* **11** 4486
- [69] Ou-Yang Z C and Helfrich W 1987 *Phys. Rev. Lett.* **59** 2486
- [70] Fernandez-Puente L, Bivas I, Mitov M and Méléard P 1994 *Europhys. Lett.* **28** 181
- [71] Patel L A and Kindt J T 2016 *Soft Matter* **12** 1765
- [72] Lai K, Wang B, Zhang Y and Zhang Y 2012 *Phys. Chem. Chem. Phys.* **14** 5744
- [73] Lai K, Wang B, Zhang Y and Zheng Y 2013 *Phys. Chem. Chem. Phys.* **15** 270